碩士學位論文

First-Order Eikonal Phase Shift Analysis for ^{16}O + ^{16}O Elastic Scatterings

濟州大學校 大學院
物理學科

文 慧 英

2001 年 12 月

$^{16}O + {}^{16}O$ 탄성산란에 대한 제 1차 Eikonal 위상이동 분석

指導敎授 金 珞 柱

文 慧 英

이 論文을 理學 碩士學位 論文으로 提出함

2001 年 12 月

文 慧 英의 理學 碩士學位 論文을 認准함

審査委員長 _____ 印
委 員 _____ 印
委 員 _____ 印

제주대학교 대학원

2001 年 12 月

First-Order Eikonal Phase Shift Analysis for $^{16}O + {}^{16}O$ Elastic Scatterings

Hye-Young Moon
(Supervised by professor Yong-Joo Kim)

A thesis submitted in partial fulfillment of the requirement for the degree of Master of Natural Sciences

2001. 12.

This Thesis has been examined and approved

.....

.....

.....

2001. 12.

DEPARTMENT OF PHYSICS
GRADUATE SCHOOL
CHEJU NATIONAL UNIVERSITY

목 차

초 록

E_{lab} = 480 과 704 MeV 에서의 ^{16}O + ^{16}O 탄성산란을 제 1차 Eikonal 위상이동을 이용하여 분석하였다. 계산결과는 실험값과 비교적 잘 일치하였다. Fuller의 포말리즘을 이용한 원측과 근측 분해를 통하여 탄성 각분포에서 보여지는 진동현상은 근측과 원측 간의 간섭현상으로 설명될 수 있었다. 고전적 편향함수를 이용하여 E_{lab} = 480 과 704 MeV 에서의 ^{16}O + ^{16}O 탄성산란 각각의 경우에 핵 무지개 현상이 존재함을 알 수 있었다. 유효 퍼텐셜과 유효 위상이동에서의 제 1차 Eikonal 보정의 역할이 논의되었다. 실수 퍼텐셜이 강하고 허수 퍼텐셜이 약할 때 허수 퍼텐셜에 대한 제 1차 Eikonal 보정 효과가 중요하다는 것을 알 수 있었다.

Ⅰ. INTRODUCTION

For the last two decades, the elastic scattering between heavy-ions has been studied by a number of people using a variety of theoretical methods, some of which are given in Chan et al. (1981), Satchler (1983), Frahn (1985), Brink (1985), Mermaz (1985), Vitturi et al. (1987), Charagi et al. (1990), Broglia et al. (1991), and Frobrich et al. (1996). Usually, the heavy-ion elastic scattering is dominated by strong absorption, with the implication that the data are only sensitive to the surface of interaction region and the optical potential required to describe the measurements is not uniquely determined. However, the angular distribution for lighter heavy-ion elastic scattering, such as $^{12}C + ^{12}C$ and $^{16}O + ^{16}O$ systems, has shown the presence of strong refractive effects with a clear signature of a nuclear rainbow phenomena (Brandan, 1988 ; Stiliaris et al., 1989). Such a behavior was identified as being a typical refraction effect generated by the nuclear rainbow. The nuclear rainbows seen in the elastic scattering angular distributions of lighter heavy-ion systems unambiguously determine the major features of the optical potential.

In recent, there has been a great deal of studies to describe the lighter heavy-ion elastic scattering. Shallow imaginary potentials are found to be essential to describe various sets of elastic scattering data for $^{12}C + ^{12}C$ and $^{16}O + ^{12}C$ at intermediate energies (Brandan, 1988). The elastic scattering data of $^{16}O + ^{16}O$ system at E_{lab} = 250, 350 and 480 MeV has been measured and analyzed within the optical model using the density-dependent folding potential (Khoa et al., 1995). Brandan and McVoy (Brandan and McVoy, 1997) made a systematic study of the optical potentials for lighter heavy-ions. They made several interesting observations, especially on the characteristics of the ratios of the imaginary to real parts of the potentials and of the imaginary to real parts of the phase shifts. Nicoli et al. (Nicoli et al., 1999) have measured the $^{16}O + ^{16}O$ elastic scattering at nine energies between E_{lab}

= 75 and 124 MeV and described in terms of phenomenological and folding model potentials which reproduce the main features observed.

The interpretation and description of scattering phenomena in heavy-ion reactions have been greatly facilitated by the application of semiclassical methods. The widely used method for the analysis of elastic scattering data is the WKB approximation (Chan et al., 1981 ; Brink, 1985 ; Donnelly et al., 1974). The eikonal phase shift is derived from the integral equation by further approximating the WKB results. Over the past several years, the eikonal approximation has been a useful tool to describe the heavy-ions elastic scattering. A number of studies (Knoll Schaeffer, 1976 ; Waxman et al., 1981 ; Silveira et al., 1987 ; Fäldt et al., 1992 ; Aguiar et al., 1997 ; Cha and Kim, 1995 ; Kim and Cha, 2000) have been made to describe elastic scattering processes between heavy ions within the framework of the eikonal model. The first- and second-order corrections to the zeroth-order eikonal phase shifts for heavy-ion elastic scatterings based on Coulomb trajectories of colliding nuclei are presented and it has been applied satisfactorily to the ^{16}O + ^{40}Ca and ^{16}O + ^{90}Zr systems at E_{lab} =1503 MeV (Cha and Kim, 1995). Eliseev and Hanna (Eliseev and Hanna, 1997) have developed first- and third-order non-eikonal corrections to the Glauber model to know the possibility of observing a bright interior in the nucleus "viewed" by intermediate energy alpha particles (E_a=172.5 MeV), as a probe for the ^{58}Ni nucleus. Aguiar et al. (Aguiar et al., 1997) have discussed different schemes devised to extend the eikonal approximation to the regime of low bombarding energies in heavy-ion collisions.

In recent, the ^{16}O + ^{16}O elastic scattering has been measured very accurately, up to large angles exhibiting down to very small cross sections and show the presence of strong refractive effects in the angular distributions (Khoa et al., 1995). It is interesting to incorporate the first-order eikonal model formalism to include refractive ^{16}O + ^{16}O elastic scattering. In this study, we analyze the elastic scatterings of ^{16}O + ^{16}O system at E_{lab} = 480 and 704 MeV by using the first-order eikonal phase shift based on Coulomb

trajectories of colliding nuclei. The presence of nuclear rainbow is examined from the semiclassical deflection function. The near-side and far-side decomposition of the elastic cross sections due to the Fuller relationship (Fuller, 1975) are presented. Some features of effective phase shift and effective potential are also investigated. In section Ⅱ, we provide the theory related with the first-order eikonal phase shift based on Coulomb trajectories of colliding nuclei and its related effective optical potential. Section Ⅲ contains results and discussions for first-order eikonal phase shift analysis. Finally, conclusions are presented in section Ⅳ.

Ⅱ. THEORY

1. Scattering Amplitude

In the case of elastic scattering between two identical spinless nuclei, the general expression of the differential cross section is given by the following formula

$$\frac{d\sigma}{d\Omega} = |f(\theta) + f(\pi - \theta)|^2. \tag{1}$$

The elastic scattering amplitude for spin-zero particles via Coulomb and short-range central forces is given by

$$f(\theta) = \frac{1}{ik} \sum_{L=0}^{\infty} (L + \frac{1}{2})(S_L - 1) P_L(\cos\theta). \tag{2}$$

Here, $k = \frac{1}{\hbar}\sqrt{2\mu E}$ is the wave number and the scattering function S_L is related to the phase shift for the L-th partial wave, and μ is the reduced mass.

Since the Coulomb interaction between heavy-ions is strong, it is convenient to separate the Coulomb contribution by writing $S_L = S_L^N \exp(2i\sigma_L)$ where $\sigma_L = \arg\Gamma(L + 1 + i\eta)$ are the Coulomb phase shifts and $\eta = \mu Z_1 Z_2 e^2/(\hbar^2 k)$ is the Sommerfeld parameter. Then, the scattering amplitude $f(\theta)$ can be separated into the Rutherford and the nuclear parts by writing (Satchler, 1983 ; Brink, 1985)

$$f(\theta) = f_R(\theta) + f_N(\theta) \tag{3}$$

where the Rutherford scattering amplitude $f_R(\theta)$ is given by

$$f_R(\theta) = -\frac{\eta}{2k\sin^2(\theta/2)} \exp[2i\sigma_0 - i\eta \ln(\sin^2\frac{\theta}{2})] \tag{4}$$

and the nuclear scattering amplitude $f_N(\theta)$ is expressed as

$$f_N(\theta) = \frac{1}{ik} \sum_{L=0}^{\infty} (L + \frac{1}{2}) \exp(2i\sigma_L)(S_L^N - 1) P_L(\cos\theta). \tag{5}$$

The nuclear scattering function S_L^N can be expressed by the nuclear phase shifts δ_L

$$S_L^N = \exp(2i\delta_L). \tag{6}$$

2. WKB Formula for the Nuclear Phase Shift

Elastic scattering phase shifts for a partial wave L are obtained by solving the Schrödinger equation

$$\frac{d^2}{dr^2} u_L(r) + k^2(r) u_L(r) = 0 \tag{7}$$

where,

$$\begin{aligned} k^2(r) &= \frac{2\mu}{\hbar^2}(E - V(r)) \\ V(r) &= U(r) + V_C(r) + \frac{\hbar^2 L(L+1)}{2\mu r^2}. \end{aligned} \tag{8}$$

In Eq.(8), $U(r)$ is the nuclear potential acting between the target and the projectile and $V_C(r)$ is the Coulomb potential. For large r, the wave function $u_L(r)$ has the asymptotic form (Brink, 1985)

$$u_L(r) \simeq \sin(kr - \eta \ln 2kr - \frac{1}{2} L\pi + \sigma_L + \delta_L). \tag{9}$$

Suppose that there is one classical turning point at r_t

$$k(r_t) = 0 \tag{10}$$

and the region $r > r_t$ is allowed classically ($E > V(r)$) and $r < r_t$ is classically forbidden ($E < V(r)$). The WKB wave function in the classically allowed region is given (Brink, 1985)

$$u_L(r) \simeq (k(r))^{-1/2} \sin\left(\int_{r_t}^{r} k(r) dr + \frac{1}{4}\pi \right). \tag{11}$$

The integral in WKB wave function can be rewritten as

$$\int_{r_t}^{r} k(r) dr = \int_{r_C}^{r} k_C(r) dr + \left[\int_{r_t}^{r} k(r) dr - \int_{r_C}^{r} k_C(r) dr \right], \tag{12}$$

where the first term is the Coulomb WKB integral and r_C is the Coulomb turning point given by

$$r_C = \frac{1}{k}\left\{\eta+\left[\eta^2+(L+\frac{1}{2})^2\right]^{1/2}\right\}. \tag{13}$$

The nuclear phase shifts can be found by combining Eq.(9) and Eq.(11) through the following relation,

$$\sin\left(kr-\frac{1}{2}L\pi-\eta\ln 2kr+\sigma_L+\delta_L\right) \simeq \sin\left(\int_{r_t}^{r}k(r)dr+\frac{1}{4}\pi\right)$$
$$= \sin\left(\int_{r_c}^{r}k_C(r)dr+\left[\int_{r_t}^{r}k(r)dr-\int_{r_c}^{r}k_C(r)dr\right]+\frac{1}{4}\pi\right). \tag{14}$$

Using the following relation

$$\sin\left(\int_{r_c}^{r}k_C(r)dr+\frac{1}{4}\pi\right) = \sin\left(kr-\frac{1}{2}L\pi-\eta\ln 2kr+\sigma_L\right), \tag{15}$$

Eq.(14) becomes

$$\sin\left(\int_{r_c}^{r}k_C(r)dr+\frac{1}{4}\pi+\left[\int_{r_t}^{r}k(r)dr-\int_{r_c}^{r}k_C(r)dr\right]\right)$$
$$= \sin\left(kr-\frac{1}{2}L\pi-\eta\ln 2kr+\sigma_L+\left[\int_{r_t}^{r}k(r)dr-\int_{r_c}^{r}k_C(r)dr\right]\right). \tag{16}$$

Therefore, WKB formula for the nuclear phase for $r\to\infty$ is given by (Chan et al., 1981 ; Brink, 1985)

$$\delta_L \simeq \int_{r_t}^{\infty}k(r)dr-\int_{r_c}^{\infty}k_C(r)dr \tag{17}$$

where,

$$k_C(r) = k\left[1-(\frac{2\eta}{kr}+\frac{(L+\frac{1}{2})^2}{k^2r^2})\right]^{1/2}, \tag{18}$$

$$k(r) = k\left[1-(\frac{2\eta}{kr}+\frac{(L+\frac{1}{2})^2}{k^2r^2}+\frac{U(r)}{E})\right]^{1/2}. \tag{19}$$

3. Eikonal Phase Shift and its First-Order Correction

In the high energy limit, we can consider the nuclear potential as a perturbation. Thus, the turning point r_t may be taken to be coincident with

r_C, and

$$k(r)-k_C(r) = k[1-(\frac{2\eta}{kr}+\frac{(L+\frac{1}{2})^2}{k^2r^2}+\frac{U(r)}{E})]^{1/2} - k[1-(\frac{2\eta}{kr}+\frac{(L+\frac{1}{2})^2}{k^2r^2})]^{1/2}$$
$$= k_C(r)\left(1-\frac{k^2U(r)}{k_C^2E}\right)^{1/2}-k_C(r). \quad (20)$$

Since wave number k is $k=\frac{1}{\hbar}\sqrt{2\mu E}$, Eq. (20) is arranged as

$$k(r)-k_C(r) = k_C(r)\left(1-\frac{2\mu U(r)}{\hbar^2k_C^2(r)}\right)^{1/2}-k_C(r)$$
$$= k_C(r)\left[1-\frac{\mu U(r)}{\hbar^2k_C^2(r)}-\frac{\mu^2U^2(r)}{2\hbar^4k_C^4(r)}-\frac{\mu^3U^3(r)}{2\hbar^6k_C^6(r)}+\cdots\right]-k_C(r)$$
$$\simeq -\frac{\mu U(r)}{\hbar^2k_C(r)}-\frac{\mu^2U^2(r)}{2\hbar^4k_C^3(r)}-\frac{\mu^3U^3(r)}{2\hbar^6k_C^5(r)}. \quad (21)$$

Thus, the nuclear phase shift δ_L in Eq. (17) can be rewritten

$$\delta_L = \int_{r_t}^{\infty}k(r)dr-\int_{r_C}^{\infty}k_C(r)dr$$
$$\simeq \int_{r_C}^{\infty}k(r)dr-\int_{r_C}^{\infty}k_C(r)dr$$
$$= \int_{r_C}^{\infty}[k(r)-k_C(r)]dr$$
$$= \int_{r_C}^{\infty}\left[-\frac{\mu U(r)}{\hbar^2k_C(r)}-\frac{\mu^2U^2(r)}{2\hbar^4k_C^3(r)}-\frac{\mu^3U^3(r)}{2\hbar^6k_C^5(r)}\right]dr$$
$$= -\frac{\mu}{\hbar^2}\int_{r_C}^{\infty}\frac{U(r)}{k_C(r)}dr-\frac{\mu}{2\hbar^4}\int_{r_C}^{\infty}\frac{U^2(r)}{k_C^3(r)}dr-\frac{\mu^3}{2\hbar^6}\int_{r_C}^{\infty}\frac{U^3(r)}{k_C^5(r)}dr \quad (22)$$

with $r=\sqrt{r_C^2+z^2}$. The first term in the above equation is the ordinary Coulomb-modified eikonal phase shift function and it can be written

$$\delta_L^0(r_C) = -\frac{\mu}{\hbar^2}\int_{r_C}^{\infty}\frac{U(r)}{k_C(r)}dr$$
$$= -\frac{\mu}{\hbar^2k}\int_{r_C}^{\infty}\frac{rU(r)}{\sqrt{r^2-r_C^2}}dr$$
$$= -\frac{\mu}{\hbar^2k}\int_{r_C}^{\infty}\frac{U(\sqrt{r_C^2+z^2})}{z}zdz$$

$$= -\frac{\mu}{\hbar^2 k}\int_0^\infty U(\sqrt{r_C^2+z^2})dz. \tag{23}$$

And the second term in Eq. (22) is the first-order correction to eikonal phase shift and it may be written

$$\begin{aligned}
\delta_L^1(r_C) &= -\frac{\mu^2}{2\hbar^4}\int_{r_C}^\infty \frac{U^2(r)}{k_C^3(r)}\,dr \\
&= -\frac{\mu^2}{2\hbar^4 k^3}\int_{r_C}^\infty \frac{r^3U^2(r)}{(r^2-r_C^2)^{3/2}}\,dr \\
&= -\frac{\mu^2}{2\hbar^4 k^3}\int_0^\infty r^2U(r)\,z^3\,dr \\
&= -\frac{\mu^2}{2\hbar^4 k^3}\int_0^\infty (1+\frac{r_C^2}{z^2})U^2(r)dz \\
&= -\frac{\mu^2}{2\hbar^4 k^3}\int_0^\infty (1+\frac{r_C^2}{z^2})U^2(r)dz \\
&= -\frac{\mu^2}{2\hbar^4 k^3}(1+r_C\frac{\partial}{\partial r_C})\int_0^\infty U^2(\sqrt{r_C^2+z^2})dz.
\end{aligned} \tag{24}$$

Summing up, the Coulomb-modified eikonal phase shift and its first-order correction are expressed following as

$$\delta_L^0(r_C) = -\frac{\mu}{\hbar^2 k}\int_0^\infty U(\sqrt{r_C^2+z^2})dz, \tag{25}$$

$$\delta_L^1(r_C) = -\frac{\mu^2}{2\hbar^4 k^3}\left(1+r_C\frac{\partial}{\partial r_C}\right)\int_0^\infty U^2(\sqrt{r_C^2+z^2})\,dz. \tag{26}$$

The first-order eikonal correction term of the phase shift, $\delta_L^1(r_C)$ in Eq. (26), can further be expressed as following

$$\delta_L^1(r_C) = -\frac{\mu^2}{\hbar^4 k^3}\int_0^\infty\left[U^2(r)+rU(r)\frac{\partial U(r)}{\partial r}\right]dz. \tag{27}$$

The closed expression of the effective phase shift function including up to the first-order correction term may be written as

$$\delta_L(r_C) = \delta_L^0(r_C)+\delta_L^1(r_C) = -\frac{\mu}{\hbar^2 k}\int_0^\infty U_{\text{eff}}(r)\,dz, \tag{28}$$

where $U_{\text{eff}}(r)$ is the effective optical potential given by

$$U_{\text{eff}}(r) = U\left\{1+\frac{\mu}{\hbar^2 k^2}\left[U+r\frac{\partial U}{\partial r}\right]\right\}. \tag{29}$$

We can see that the eikonal phase shift calculation including the first-order correction is equivalent to a zeroth-order calculation with effective potential

$U_{\text{eff}}(r)$. By taking $U(r)$ as the squared Woods-Saxon forms given by

$$U(r) = -\frac{V_0}{(1+e^{(r-R_v)/a_v})^2} - i\frac{W_0}{(1+e^{(r-R_w)/a_w})^2}, \tag{30}$$

with $R_{v,w} = r_{v,w}(A_1^{1/3} + A_2^{1/3})$, we can use the phase shifts, Eqs. (25)-(26) in the general expression for the elastic scattering amplitude, Eqs. (1) and (2).

Ⅲ. RESULTS AND DISCUSSIONS

1. Elastic Scattering Cross Section

As in the preceding section, the Coulomb-modified eikonal phase shifts δ_L^0 and δ_L^1 have been used to calculate the elastic differential cross sections for $^{16}O + ^{16}O$ system at E_{lab} = 480 and 704 MeV. Table 1 shows the parameters of the fitted Woods-Saxon squared potential. The six potential parameters are adjusted so as to minimize the χ^2/N given by

$$\chi^2/N = \frac{1}{N}\sum_{i=1}^{N}\left[\frac{\sigma^i_{\exp} - \sigma^i_{cal}}{\triangle\sigma^i_{\exp}}\right]^2. \qquad (31)$$

In Eq. (31), $\sigma^i_{\exp}$ (σ^i_{cal}) and $\triangle_{\exp}$ are the experimental (calculated) cross sections and uncertainties, respectively, and N is the number of data used in the fitting. The calculated results of the differential cross sections for the elastic scattering of $^{16}O + ^{16}O$ system at E_{lab} = 480 and 704 MeV are presented in Figs.1 and 2 together with those measured experimentally (Khoa et al., 1995 ; Khoa et al., 2000). In Fig. 1 and Fig. 2, the solid curves are the results for the first-order eikonal phase shifts, while the dashed curves are the results of the zeroth-order eikonal phase shifts. As seen in these figures, there are the substantial differences between the dashed and solid curves when compared to the experimental results. The first-order eikonal model reproduce the characteristic refractive patterns observed experimentally. The calculated angular distributions are nearly identical at forward angles but are qualitatively different at large angles. As a whole, our calculations lead to reasonable predictions over the whole angular range for the elastic scattering data in the $^{16}O + ^{16}O$ system at E_{lab} = 480 and 704 MeV, respectively. Also, the reasonable χ^2/N values are obtained in the $^{16}O + ^{16}O$ system at E_{lab} = 480 and 704 MeV, respectively, as listed in table 1.

TABLE 1: Parameters of the fitted Woods-Saxon squared potential by using the first-order eikonal phase shift analysis for the ^{16}O + ^{16}O elastic scattering at E_{lab} = 480 and 704 MeV. 10% error bars are adopted to obtain χ^2/N value.

Energy	V_0	r_v	a_v	W_0	r_w	a_w	R_S	σ_{R_S}	σ_R	χ^2/N	
(MeV)	(MeV)	(fm)	(fm)	(MeV)	(fm)	(fm)	(fm)	(mb)	(mb)	δ^0	$\delta^0+\delta^1$
480	233	0.897	1.299	55.4	1.107	1.275	7.04	1558	1626	11.61	6.10
704	278	0.894	1.370	48.9	1.186	0.903	6.76	1437	1469	8.71	5.88

In order to understand the nature of angular distributions for ^{16}O + ^{16}O system at E_{lab} = 480 and 704 MeV, the near- and far-side decompositions of scattering amplitudes are also performed with the first-order correction to the eikonal phase shifts by following Fuller's formalism (Fuller, 1975). The contributions of the near- and far-side components to the elastic scattering cross sections are shown in Fig. 3 along with the differential cross sections. The differential cross section is not just a sum of the near- and far-side cross sections but contains the interference between the near- and far-side amplitudes as shown in Fig. 3. The oscillations observed on the elastic scattering angular distributions of ^{16}O + ^{16}O system at E_{lab} = 480 and 704 MeV are due to the interferences between the near- and far-side components. The magnitudes of the near- and far-side contributions are equal, crossing point, at $\theta = 8.4^\circ$ for E_{lab} = 480 MeV and $\theta = 4.8^\circ$ for E_{lab} = 704 MeV, respectively. Figure 3 shows the near-side dominance at angles less than these values due to the long-range repulsive Coulomb interaction. However, the far-side contributions to the cross sections have become dominant at the regions greater than the crossing angles due to the short-range attractive nuclear interaction.

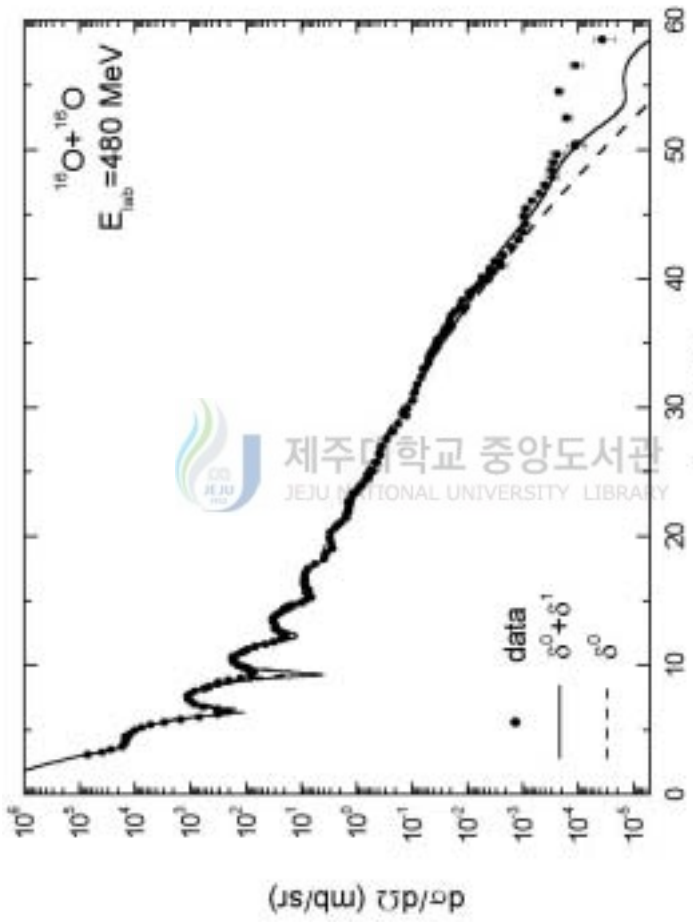

FIG. 1: Elastic scattering angular distributions for $^{16}O+^{16}O$ system at E_{lab} = 480 MeV. The solid circles denoted the observed data taken from Khoa et al.(1995). The solid and dashed curves are the results for the first- and zeroth-order eikonal corrections, respectively.

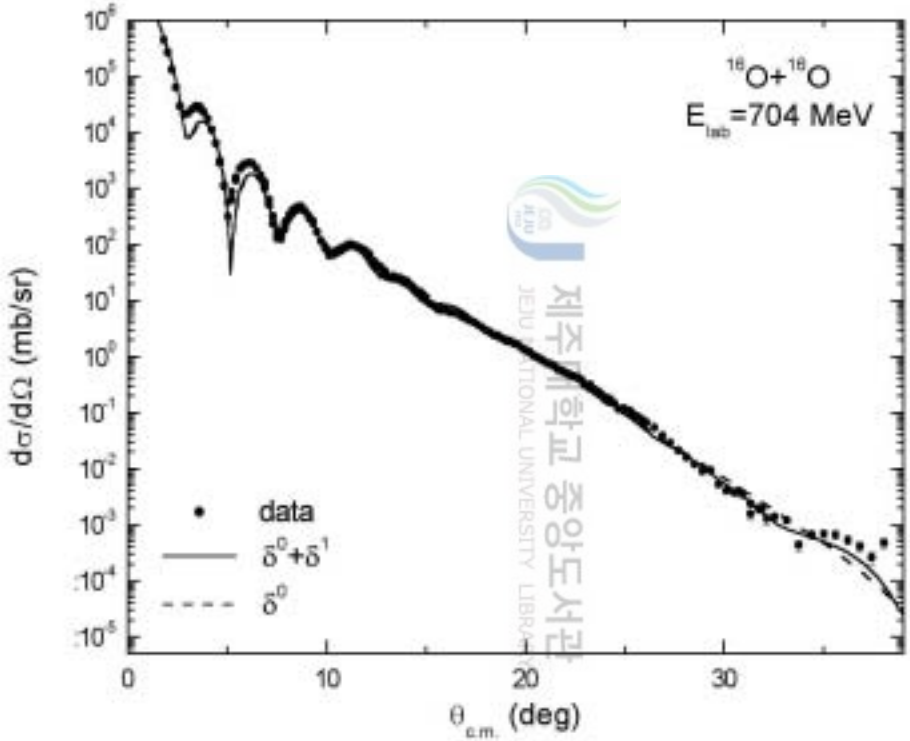

FIG. 2: Elastic scattering angular distributions for $^{16}O+^{16}O$ system at E_{lab} = 704 MeV. The solid circles denoted the observed data taken from Khoa et al.(2000). The solid and dashed curves are the results for the first- and zeroth-order eikonal corrections, respectively.

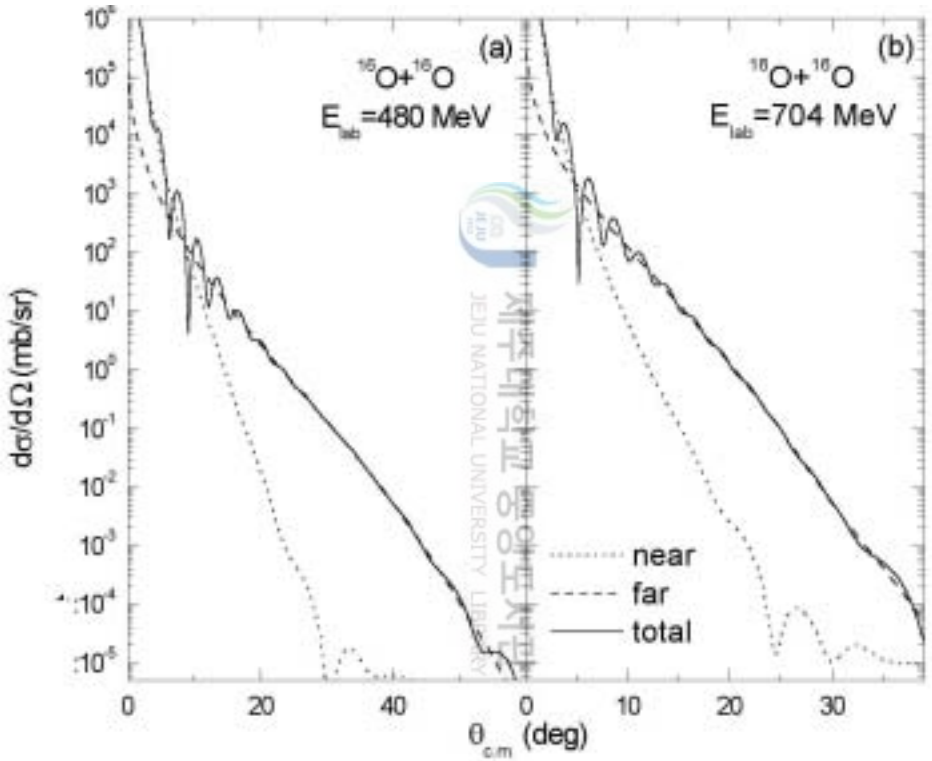

FIG. 3: Differential cross sections (solid curves), near-side contributions (dotted curves), and far-side contributions (dashed curves) obtained by the Fuller's formalism(Fullar, 1975) using the first-order eikonal model for $^{16}O+^{16}O$ system at E_{lab} = 480 and 704 MeV.

2. Deflection Function and Nuclear Rainbow

It is known that when the absorptive potential is weak and the real potential is strong, the contributions to the scattering from the interior region are large enough to be observed. In analogy to optics, these contributions are called refractive, since the scattered particles have partially penetrated the target nucleus. This situation is interpreted as "nuclear rainbow scattering", because the intensity maximum is built by many trajectories being essentially deflected the same scattering angle; the nuclear rainbow angle θ_{nr}. The nuclear rainbow angle is obtained from the classical deflection function given by

$$\theta_L = 2\frac{d}{dL}(\sigma_L + \mathrm{Re}\,\delta_L). \quad (32)$$

This deflection angle is a semiclassical treatment of a trajectory with angular momentum L and calculated from the Coulomb phase σ_L and real nuclear phase δ_L.

The term "nuclear rainbow" shows the differential cross section for scattering to the negative angles from the far-side component of the target. In a rainbow situation, the strong nuclear force attracts the projectiles towards the scattering center and deflects them to negative scattering angles, which correspond to the region of the rainbow maximum. As shown in table 1, the absorption in $^{16}O + ^{16}O$ system is weak enough to allow refracted projectiles to populate the elastic channel and typical nuclear rainbow effects could be observed in the angular distribution. In Fig. 4, we can find the nuclear rainbow angle values $\theta_{nr} = -42.6^\circ$ and $\theta_{nr} = -32.7^\circ$ for the $^{16}O + ^{16}O$ system at E_{lab} = 480 and 704 MeV, respectively, which evidently prove a presence of the nuclear rainbow with unambiguous clarity in this system. It can be notice that the nuclear rainbow angle values decrease as the incident energy increases. Such a behavior seems to correspond to the incident energy and the ratio of the imaginary to real part of a scattering potential.

3. Transmission Function and Partial Wave Reaction Cross Section

The transmission function $T_L = 1 - |S_L|^2$ is plotted versus the orbital angular momentum in Fig. 5 along with the partial wave reaction cross section σ_L for $^{16}O + ^{16}O$ system at E_{lab} = 480 and 704 MeV, respectively. Transmission function can be explained using the imaginary part of the effective optical potential. As shown Fig. 5(a), the lower partial waves are totally absorbed and the T_L is decreased very rapidly in a narrow localized angular momenta zone.

We can see in Fig. 5(b) that the values of the partial reaction cross section increase linearly up to L= 55 for E_{lab} = 480 MeV and L= 66 for E_{lab} = 704 MeV, respectively. Beyond these L-values, the partial reaction cross sections decrease quadratically. A further investigation of the situation can be gained by looking at the strong absorption radius (R_S) and the reaction cross section (σ_{R_S}) given in table 1. The strong absorption radius is defined as the distance for which $T_L = 1/2$, i.e., the distance where the incident particle has the same probability to be absorbed as to be reflected. The strong absorption radius provides a good estimate of the reaction cross section, $\sigma_{R_S} = \pi R_S^2$.

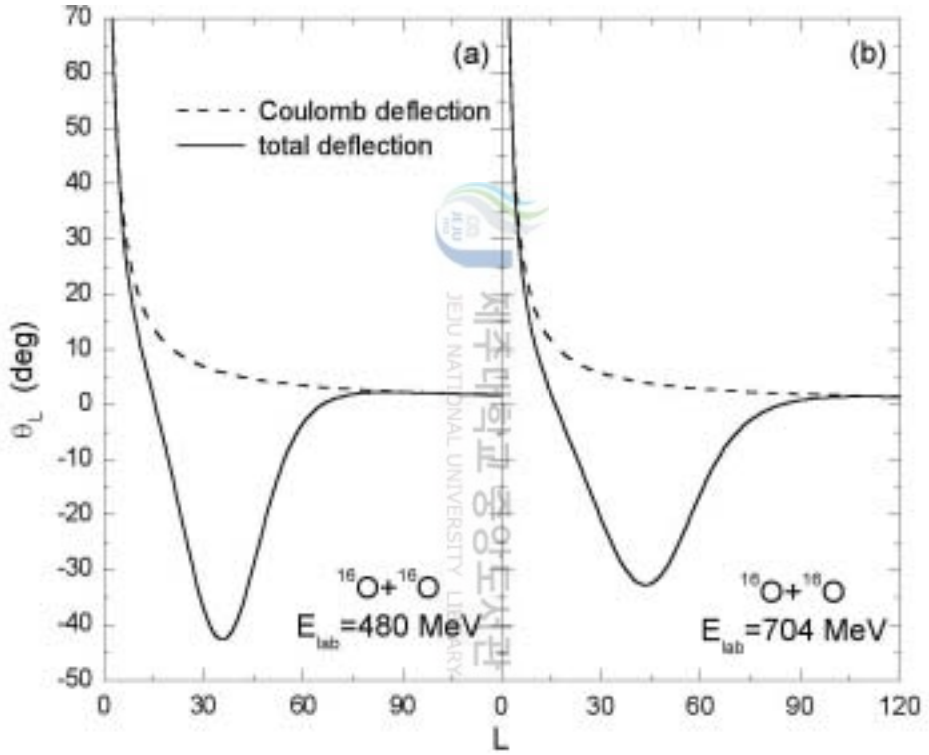

FIG. 4: Deflection Functions for $^{16}O+^{16}O$ system at E_{lab} = 480 and 704 MeV plotted versus the orbital angular momentum L in the first-order eikonal model. The dashed curve represents the deflection function for the Coulomb phase shift.

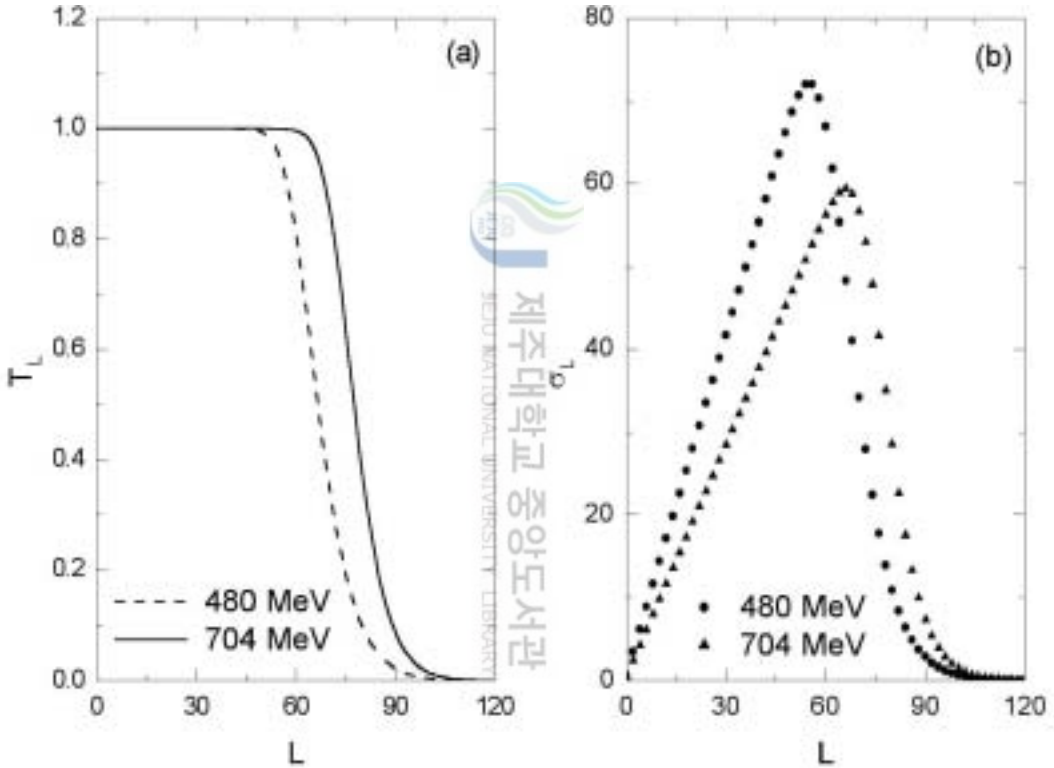

FIG. 5: (a) Transmission functions T_L and (b) Partial wave reaction cross sections σ_L for $^{16}O+^{16}O$ system at E_{lab} = 480 and 704 MeV plotted versus the orbital angular momentum L.

4. Effective Potential

In order to illustrate the differences between the effective and nominal potentials, we plot the real and imaginary parts of these potentials in Fig. 6 and Fig.7. In these figures, the solid curves are the real and imaginary parts of effective potentials U_{eff} given in Eq. (29), while the dashed curves are the real and imaginary parts of the nominal potentials $U(r)$ given in Eq. (30). As shown in these figures, there is a dramatic difference between the two potentials, especially for the imaginary part. We can see in Eq. (29) that the effective imaginary potential with the first-order eikonal correction depends on the product of the real and imaginary potentials and their derivatives. Thus the effective imaginary potentials rapidly increase until they reach maximum value in the central region of the nucleus, and then they reach minimum in the surface region. A drastic increase of the imaginary potential for small values of r corresponding to increased transmission is mainly due to the correction term in Eq. (29). In the traditional eikonal model, it is assumed that the imaginary part of the potential is responsible for the absorption process in the nuclear reaction and its shape should not be affected by the real part. Nevertheless, in the present eikonal model with the first-order correction, we can find that the drastic increase on the absorptive potential in the small r region are due to the larger real potential compared with imaginary one.

In the small r region, the effective imaginary potential of the first-order eikonal model is small compared with the effective real potential. Such a small ratio makes it possible to interpenetrate each other between the projectile and target nuclei. As a result, the projectile ion can penetrate the nuclear surface barrier of the target, and the cross section becomes sensitive to the value of the real potential in the central region.

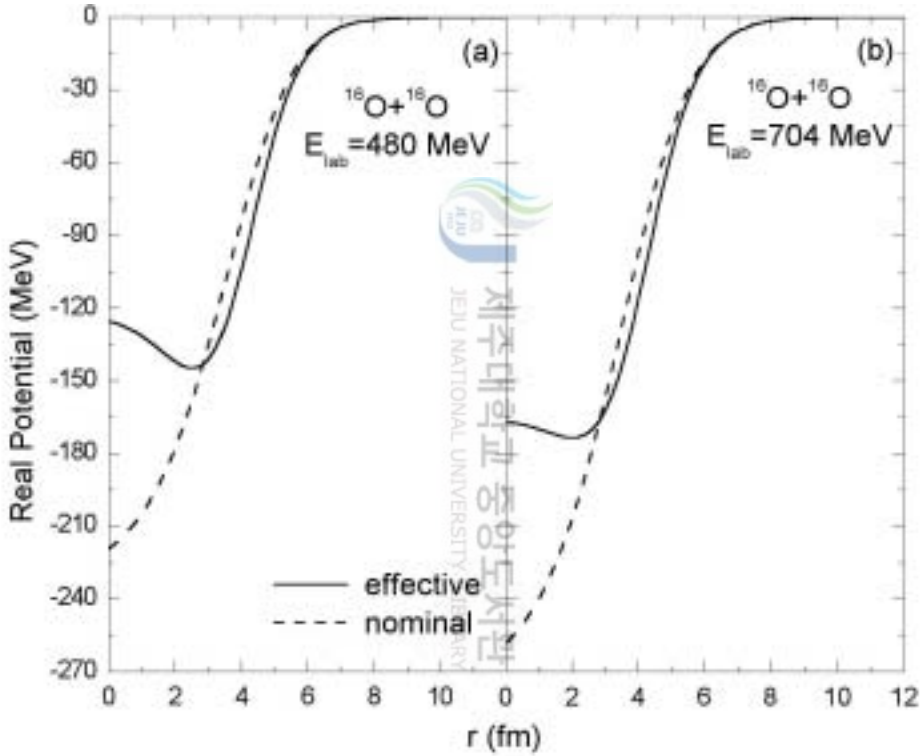

FIG. 6: Real parts of the effective potential $^{16}O+^{16}O$ system at E_{lab} = 480 and 704 MeV. The solid and dashed curves are the results for first- and zeroth-order eikonal corrections, respectively.

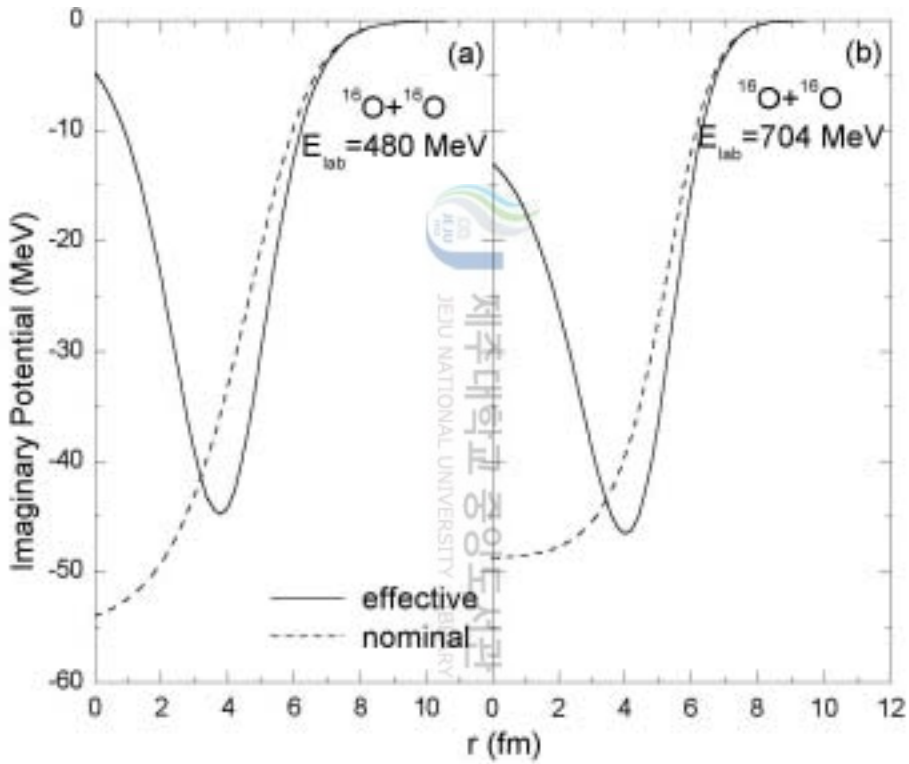

FIG. 7: Imaginary parts of the effective potential $^{16}O+^{16}O$ system at E_{lab} = 480 and 704 MeV. The solid and dashed curves are the results for first- and zeroth-order eikonal corrections, respectively.

5. Effective Phase Shift

Such increase of the effective potential in the small r regions are also reflected in the phase shift function. Fig. 8 and Fig. 9 show the angular momentum dependence of the real and imaginary parts of zeroth- and first-order eikonal phase shift. The solid curves are the phase shifts of first-order eikonal model, while the dashed curves are the results of the ordinary eikonal model. On the whole, the real phase shifts vanish nearly quadratically as the L increase. The real phase shifts of the first-order eikonal corrections are less values than the results of zero-order eikonal phase shifts at $L < 17$ for E_{lab} = 480 MeV and $L < 21$ for E_{lab} = 704 MeV, however, are greater ones at these L values for E_{lab} = 480 and 704 MeV, respectively. However, we can see that the real potential gives a drastic change of the imaginary phase shifts. In Fig. 9, the dramatic variations of imaginary phase shifts are found in the first-eikonal corrections, as expected. We can also see in the imaginary phase shifts of the first-order eikonal corrections are less values at $L < 20$ and $L < 27$ compared to the results of zeroth-order eikonal phase shifts, however greater ones at these L values for E_{lab} = 480 and 704 MeV, respectively. The strong absorption in the nuclear surface plays a dominant role to the scattering amplitude and thus to the characteristic diffraction pattern of the angular distribution. The large angle behavior is sensitive to the details of the real optical potential over a wide radial region from the nuclear surface towards the interior.

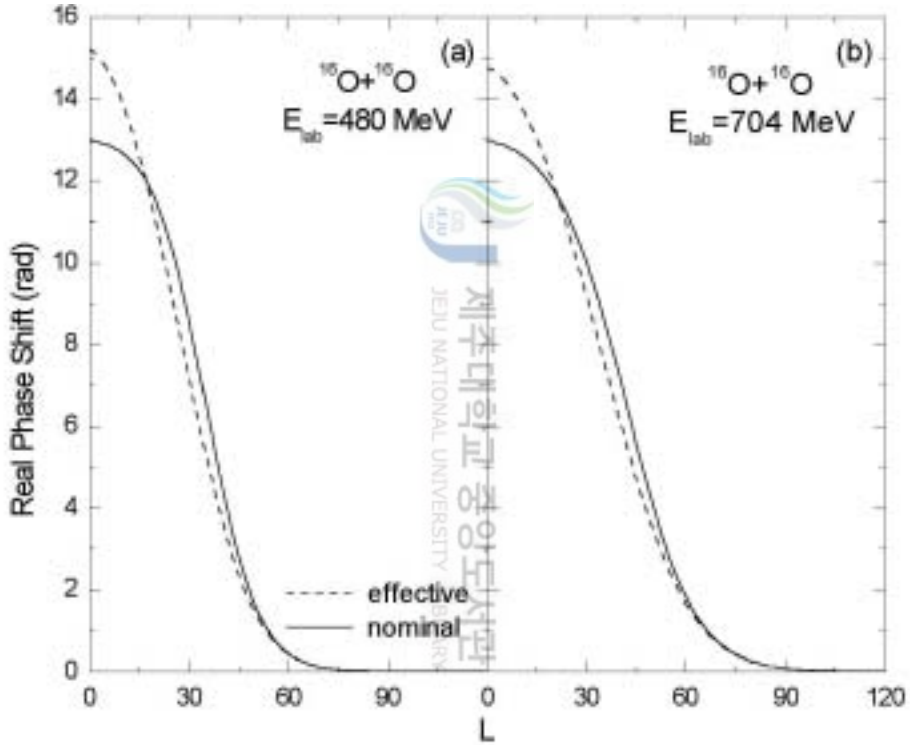

FIG. 8: Real parts of the effective phase shifts $^{16}O+^{16}O$ system at E_{lab} = 480 and 704 MeV. The solid and dashed curves are the results for first- and zeroth-order eikonal corrections, respectively.

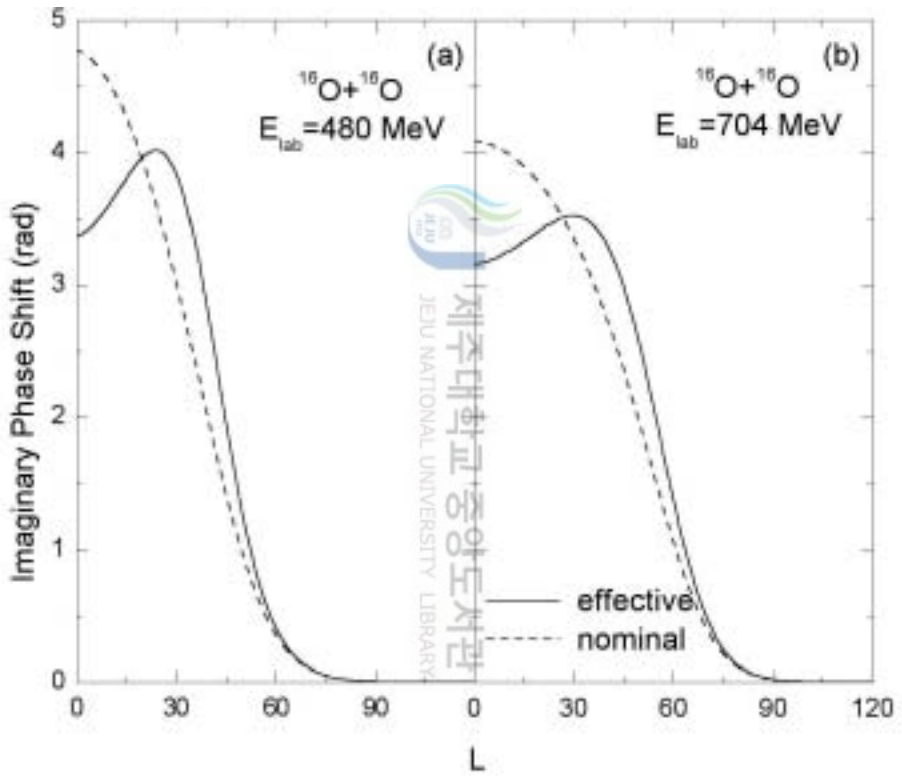

FIG. 9: Imaginary parts of the effective phase shifts $^{16}O+^{16}O$ system at E_{lab} = 480 and 704 MeV. The solid and dashed curves are the results for first- and zeroth-order eikonal corrections, respectively.

Ⅳ. CONCLUSIONS

In this study, we have analyzed the elastic scatterings of $^{16}O + ^{16}O$ system at E_{lab} = 480 and 704 MeV by using the first-order eikonal phase shift based on the Coulomb trajectories of colliding nuclei and squared Woods-Saxon potential. We have found that the calculated results using the first-order eikonal phase shift are reasonable agreements with the observed data in this system. Through near- and far-side decompositions of the cross section, we have shown that the oscillations of $^{16}O + ^{16}O$ system are due to the interferences between the near- and far-side amplitudes. All of cases show near-side dominance from the long-range repulsive Coulomb interaction at forward angles and far-side dominance from the short-ranged attractive nuclear interaction at large angles. We have obtained the nuclear rainbow angle values $\theta_{nr} = -42.6^\circ$ and $\theta_{nr} = -32.7^\circ$ for the $^{16}O + ^{16}O$ system at E_{lab} = 480 and 704 MeV, respectively, through a classical deflection function, and they evidently prove a presence of the nuclear rainbow in this system. The nuclear rainbow angle value decreases as the incident energy increases in this system. The partial reaction cross section increase linearly up to $L = 55$ for E_{lab} = 480 and $L = 66$ for E_{lab} = 704 MeV, respectively. Beyond this L value, the partial reaction cross sections have decrease quadratically. Furthermore, the strong absorption radius provides a good estimate of the reaction cross section, $\sigma_{R_s} = \pi R_S^2$.

The strongly real and weakly imaginary optical potentials are found and they support the presence of nuclear rainbows in the angular distribution of this system. We have also found that the effect of first-order eikonal correction on the imaginary potential is important in this case. The strongly real potential give a drastic effect on the effective imaginary potential for $^{16}O + ^{16}O$ system at E_{lab} = 480 and 704 MeV, respectively. The ratio of imaginary to real part of effective potential is very small in the central region

and such a small ratio value makes it possible to interpenetrate each other between the projectile and target nuclei. The refractive part, dominated by the far-side component of the scattering amplitude is sensitive to the real heavy-ion optical potential at small radii. The imaginary effective potential of first-order eikonal model have pronounced minimum between central and surface regions of nucleus, while the nominal imaginary potential increase monotonically. Such effective potentials are reflected in the phase shift functions. The strongly real potential give a drastic effect on the imaginary phase shifts for ^{16}O + ^{16}O system at E_{lab} = 480 and 704 MeV, respectively. We can also see in the imaginary phase shift calculated with the real potential that an absorption of partial waves for large angular momentum increases, whereas the absorption decreases for small angular momentum, compared to the result without the real potential. The strong absorption in the nuclear surface plays a dominant role to the scattering amplitude and thus to the characteristic diffraction pattern of the angular distribution. The large-angle behavior is sensitive to the details of the real optical potential over a wide radial region from the nuclear surface towards the interior.

REFERENCES

Aguiar C. E., F. Zardi and A. Vitturi, Phys. Rev. C **56**, 1511 (1997).

Brandan M. E., Phys. Rev. Lett. **60**, 784 (1988).

Brandan M. E. and K. W. McVoy, Phys. Rev. C **55**, 1362 (1997).

Brink D. M., *Semi-Classical Methods for Nucleus-Nucleus Scattering*, (Cambridge Univ. Press, Cambridge,1985)

Broglia R. A. and A. Winther, *Heavy Ion Reaction*s, (Addision-Wesley Pub. Comp., 1991).

Cha M. H. and Y. J. Kim, Phys. Rev. C **51**, 212 (1995).

Chan C. K., P. Suebka and P. Lu P, Phys. Rev. C **24**, 2035 (1981).

Charagi S. K. and S. K. Gupta, Phys. Rev. C **41**, 1610 (1990).

Donnelly T. W., J. Dubach and J. D. Walecka, Nucl. Phys. **A232**, 355 (1974).

Eliseev S. M. and K. M. Hanna, Phys. Rev. C **56**, 554 (1997).

Fäldt G., A. Ingemarsson and J. Mahalanabis, Phys. Rev. C **46**, 1974 (1992).

Frahn W. E., *Diffractive Processes in Nuclear Physics* (Oxford Univ. Press, Oxford, 1985).

Frobrich P. and R. Lipperheide, *Theory of Nuclear Reactions*, (Oxford Univ. Press, Oxford, 1996).

Fuller R. C., Phys. Rev. C **12**, 1561 (1975).

Khoa D. T., W.von Oertzen, H. G. Bohlen, G. Bartnitzky, H. Clement, Y. Sugiyama, B. Gebauer, A. N. Ostrowski, Th. Wilpert and C. Langner, Phys. Rev. Lett. **74**, 34 (1995).

Khoa D. T., W. von Oertzen, H. G. Bohlen and F. Nuoffer, Nucl. Phys. **A672**, 387 (2000).

Kim Y. J. and M. H. Cha, Int. J. Mod. Phys. **E9**, 67 (2000).

Knoll J. and R. Schaeffer, Ann. Phys. (N.Y.) **97**, 307 (1976).

Mermaz M. C., Z. Phys. **A321**, 613 (1985).

Nicoli M. P., F. Haas, R. M. Freeman, N. Aissaoui, C. Beck, A. Elanique, R. Nouicer, A. Morsad, S. Szilner, Z. Basrak, M. E. Brandan, and G. R. Satchler, Phys. Rev. C **60** 064608 (1999).

Satchler G. R., *Direct Nuclear Reactions*, (Oxford Univ. Press, Oxford (1983)).

Da Silveira R. and Ch. Leclercq-Willain, J. Phys. G **13**, 149 (1987).

Stiliaris E., H. G. Bohlen, P. Fröbrich, B. Gebauer, D. Kolbert, W. von Oertzen, M. Wilpert and Th. Wilpert, Phys. Lett. **223**, 291 (1989).

Vitturi A. and F. Zardi, Phys. Rev. C **36**, 1404 (1987).

Waxman D., C. Wilkin, J. F. Fermond and R. J. Lombard, Phys. Rev. C **24**, 578 (1981).

감사의 글

이런 저런 욕심을 가지고 대학원 생활을 시작했었던 게 바로 엊그제 같은데, 벌써 학위 논문을 마치게 되었습니다.

무엇보다도 지도교수님으로서 대학원 생활 내내 저를 이끌어 주신 김용주 교수님께 감사의 말씀을 드리고 싶습니다. 너무나도 부족했었던 제가 무사히 학위 논문을 마칠 수 있었던 건 바로 교수님의 격려와 배려 덕분이었습니다. 그리고, 심사위원으로서 저의 학위논문이 좀 더 완성된 모습이 될 수 있도록 지도해주셨던 홍성락 교수님과 현남규 교수님께도 감사의 말씀 드리고 싶습니다.

저의 학위취득을 그 누구보다도 기뻐해 주실 부모님! 당신 몸이 더 불편하심에도 불구하고 누구보다도 저의 건강과 대학원생활을 염려해주신 어머니를 생각하면, 그 고마움 어떻게 보답해드려야 될지 정말 막막하기만 합니다.

2년여의 대학원 생활을 하면서 느낀 건 바로 의식이 항상 깨어 있어야 한다는 것이었습니다. 그러나, 그 생각을 제대로 실천하지 못해 2년여의 생활에 대해 너무 커다란 아쉬움이 남습니다. 그 커다란 아쉬움만큼이나 앞으로 저의 삶이 좀 더 발전된 모습이었으면 합니다.